Markov Model for the Flow of Nanobots in the Human Circulatory System

Jorge Torres Gómez
TU Berlin, Germany
torres-gomez@ccs-labs.org

Regine Wendt
Universität zu Lübeck, Germany
wendt@itm.uni-luebeck.de

Anke Kuestner
TU Berlin, Germany
anke.kuestner@ccs-labs.org

Ketki Pitke
TU Berlin, Germany
pitke@ccs-labs.org

Lukas Stratmann
TU Berlin, Germany
stratmann@ccs-labs.org

Falko Dressler
TU Berlin, Germany
dressler@ccs-labs.org

ABSTRACT

Recent advances in nanotechnology show possible applications of nano-devices within the human body. For example, technical solutions are under development to make use of nanobots to carry and release drugs via the circulatory system. In this scenario, it is important to study the location and the location distribution of nanobots in the human circulatory system (HCS). However, due to bifurcations and the variety of structures in the human vessels, this problem is rather challenging. In this paper, we address a new methodology based on a Markov chain model to study the distribution of nanobots in the HCS. The transition probabilities are assessed through analogies of their representation with an electric circuit representation of the HCS. Additionally, we conducted simulations in the simulation framework BloodVoyagerS to compare results with the provided Markov model. Our evaluation shows that the new model accounts well for the location of the nano-devices as well as their trajectories.

KEYWORDS

Human Circulatory System, Electric Circuits, Nanobots, Markov Model

ACM Reference Format:
Jorge Torres Gómez, Regine Wendt, Anke Kuestner, Ketki Pitke, Lukas Stratmann, and Falko Dressler. 2021. Markov Model for the Flow of Nanobots in the Human Circulatory System. In *The Eight Annual ACM International Conference on Nanoscale Computing and Communication (NANOCOM '21), September 7–9, 2021, Virtual Event, Italy*. ACM, New York, NY, USA, 7 pages. https://doi.org/10.1145/3477206.3477477

1 INTRODUCTION

The development of new mechanisms for targeted drug delivery is a focus of attention in medicine and pharmaceutics with groundbreaking designs. Considering the poor pharmacokinetic properties of most therapeutic drugs (about 95 %) [2], more efficient solutions are strongly needed. Through nano-devices traveling in the blood vessels, the release of drugs is targeted to specific regions without affecting healthy tissues around [12] – this becomes particularly interesting when interconnecting these nanobots [1, 5]. Such nano-devices carry drugs of a size larger than the pores in the capillaries (2–4 nm) but less than the vascular ones concerning the solid tumors (380–780 nm), which make them ideal candidates to reach specific tumors avoiding healthy tissues.

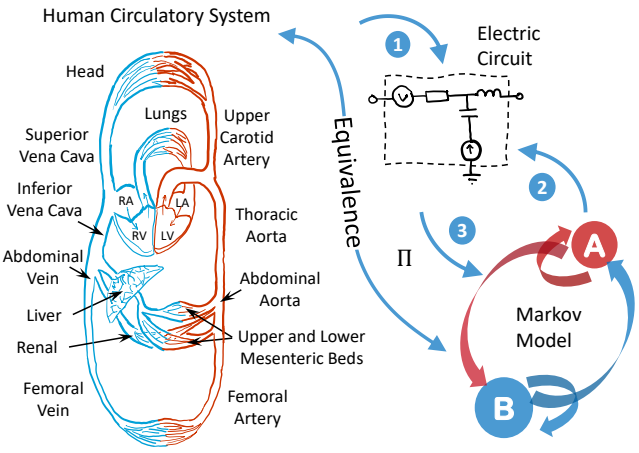

Figure 1: Methodology to derive the Markov model of the human circulatory system.

To reach a given target through the human circulatory system (HCS), nano-devices are guided by passive means driven by the direction of the blood flow, and by active means driven by external sources to the human body. For instance, polyethylene glycol (PEG)-grafted liposome nanocarriers are used for passive drug delivery to allow their circulation for a longer period of time, such as 45 h, increasing their chance of reaching the target [12]. More complex technologies are also conceived to interchange communications of nanobots with external devices to the human body through their active guiding process to the target [4, 15].

In this paper, we elaborate on a methodology to derive the location of nanobots through their passive displacement through the HCS. Guided by the blood flow, their location in the human body is random due to the bifurcations in the vessels and variable pressure and flow on each vessel segment. Instead of characterizing the flow of nanobots between release and target locations only [3], we analyze the flow of nanobots around the complete body when traveling through its closed loops.

NANOCOM '21, September 7–9, 2021, Virtual Event, Italy

ACM ISBN 978-1-4503-8710-1/21/09…$15.00
https://doi.org/10.1145/3477206.3477477

To address such a problem, we rely on the Markov chain model as a theoretical framework to study the evolution of the nanobots' position inside the human body. As depicted in Fig. 1, we elaborate on the analogies between the circuit representation of Markov chains and the electric-circuit models of the HCS to derive the corresponding transition probabilities of nano-devices in three main steps.

This methodology represents a simple and approximate method to overcome the difficulties in the measurement of the transition probabilities when modeling the HCS. By this procedure, the transition probabilities are derived relying on the well-established schemes regarding the electric-circuit representation [18] instead of more difficult approaches such as autopsy data sets [16].

Furthermore, we also provide results in the framework simulator BloodVoyagerS to account for the real-time modeling of the flowing nanobots [7, 13]. Considering the different vessel segments and their connections modeled by the Markov chain, we implement the same structure in BloodVoyagerS to obtain the distribution of nanobots per vessel segment. The derived results match pretty well with the obtained distribution through the Markov chain model.

Our main contributions can be summarized as follows:

- We developed a Markov chain-based methodology to derive probabilistic location information of nanobots in the circulatory system (Section 2);
- we also implemented the model in the BloodVoyagerS simulator to validate our analytical results (Section 2.4); and
- we present results regarding the transition probabilities, the dynamic of inserted nanobots in the blood flow, and their average location in the human body (Section 3).

2 METHODOLOGY

Our methodology consists of three different steps to derive the transition probabilities of the equivalent Markov chain for the HCS. It relies on the analogies in representing the HCS by electric circuits and by weighted circuits of the equivalent Markov chain. The three steps are as following: (1) Obtaining the electric circuit representation of the HCS (Section 2.1); (2) obtaining the weighted circuit regarding the equivalent Markov chain for the HCS, relying on the reported electric circuit in [17, 19] (Section 2.2); and (3) derivation of the relations between the transition probabilities in the Markov Chain and the electric current flows in the electric circuit representation (Section 2.3). The abbreviations used in the next sections are summarized as follows:

AbA abdominal aorta
AsA ascending aorta
AVC abdominal vena cava
CGS centimetre–gram–second system
FA femoral artery
FV femoral vein
HCS human circulatory system
HSV head small veins
JV jugular vein
KIDN kidney
LAR leg arterioles
LCAP leg capillaries
LM lower mesenteric
LOC lower carotid artery
LSA leg small artery
LSV leg small vein
LV left ventricle
LVE leg venules
PEG polyethylene glycol
RA right atrium
SI international system
SVC superior vena cava
ThA thoracic aorta
TVC thoracic vena cava
UM upper mesenteric
UPC upper carotid artery

2.1 Electric Circuit Model

The HCS can be modeled through analog electric circuits to benefit from a reduced complexity when representing their main loops. Pressure and flow in the blood are computed through voltage and currents in the equivalent analog electric circuit representation. Segments in arteries, capillaries, and veins are represented by the connection of electric elements like resistors, capacitors, and inductors to account for mechanical parameters such as viscosity, compliance, and inertia in the human vessels, respectively [18].

To implement the design, we interconnect two reported schemes. Due to the accuracy in the obtaining of pressure and flow in the heart, we use a scheme regarding the circulation of the heart and the lungs [10]. For the systemic circulation, we use the multi-component design implementation reported in [17, 18].

The scheme in [10] is implemented in Matlab/Simulink through adders, multipliers, and threshold blocks. The ventricular and atrial pressures in the right and left portion of the heart are connected to the lungs and the systemic circulation as mono-component designs. That is, the systemic circulation is implemented as a block without considering the different segments in the HCS.

To account for a multi-component design regarding the systemic circulation, the work in [17, 19] divides the HCS into four major anatomical divisions to account for the head, thorax, abdomen, and legs through the circuits' schemes depicted in Fig. 2. In this design, arteries, capillaries, and veins are represented by different circuit models according to the variety of segments.

The arteries are divided in seven segments represented by the connection of RC circuits in the L-inverted topology. Concerning the upper body they account for the lower carotid artery (LOC) through S_4 and the upper carotid artery (UPC) through S_5 in the ascending aorta (AsA), in the thorax the thoracic aorta (ThA) through S_{10}, in the abdomen the abdominal aorta (AbA) through S_{11}, and the legs by S_{12}, S_{13}, S_{14} corresponding to the femoral artery (FA), leg small artery (LSA), and the leg arterioles (LAR), respectively.

The capillaries are represented through RC circuits connected with a resistor in series, or through L and T topologies. Their connections account for the head, liver, upper mesenteric (UM), lower mesenteric (LM), kidney (KIDN) and the leg capillaries (LCAP) corresponding to seven regions represented within S_2, S_6, S_{15}, S_{16}, S_{17}, S_{18}, and S_{19} blocks.

Finally, the loop to the heart is closed through the veins. In the upper body they are given by the head small veins (HSV) in S_7,

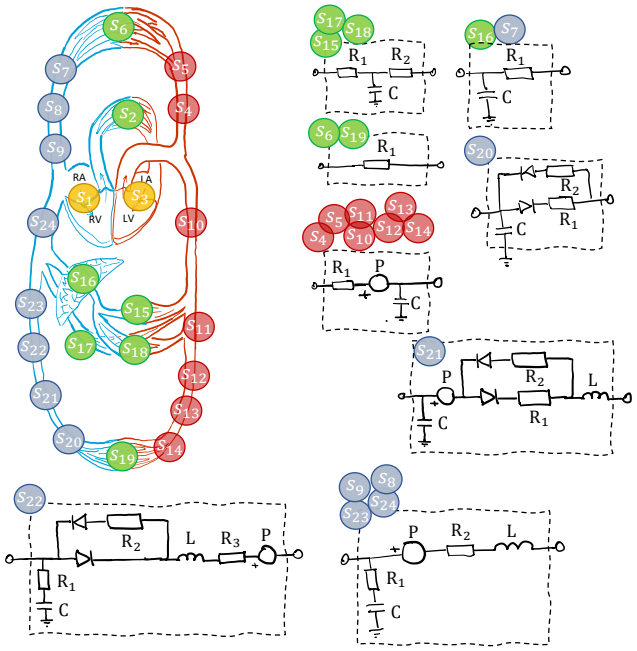

Figure 2: Electric-circuit model concerning the systemic circulation.

jugular vein (JV) in S_8, and the superior vena cava (SVC) in S_9. In the thorax region the thoracic vena cava (TVC) in S_{24}, in the abdomen the abdominal vena cava (AVC) in S_{23}, and in the legs the femoral vein (FV), leg small vein (LSV), and leg venules (LVE) represented by S_{20}, S_{21}, and S_{22}, respectively.

Additionally, in the arteries and veins supplemental voltage sources are included to account for the pressure produced by gravity. According to [19], the value of the voltage source is given as $P = nG\rho L \sin\theta$, where n is the total number of g's of acceleration, G is the acceleration due to the earth gravity, ρ is the blood viscosity, θ is the angle between the vessel segment and a perpendicular to the ground floor, and L is the segment length.

These two designs are connected in Simulink as illustrated in Fig. 3. The design in [10], for the heart-lungs circulation, is implemented in the blocks S_1 to S_3, including their connection to the systemic circulatory system block. The design in [17, 19], to account for the systemic circulation only, is implemented through the blocks S_4 to S_24 with the electric components specified in Fig. 2. Both designs are connected by pressure signals regarding the left ventricle (LV) and the right atrium (RA) compartments in the heart. The pressure's signals P_LV and P_RA – equivalently referred to as voltage – are connected to electric source voltages blocks represented by the V_RA and V_LV blocks, which in turn allows the isolation of the two designs regarding their respective electric loads. In addition, sensors for voltages (blocks with prefix P_) and currents (blocks with prefix F_) are connected to measure the pressure and flow on each segment, respectively. Finally, in the design an additional voltage source connected to the legs (denoted by P_m in Fig. 3) is also represented. This accounts for additional pressure from the leg muscles when standing up or during walking [19].

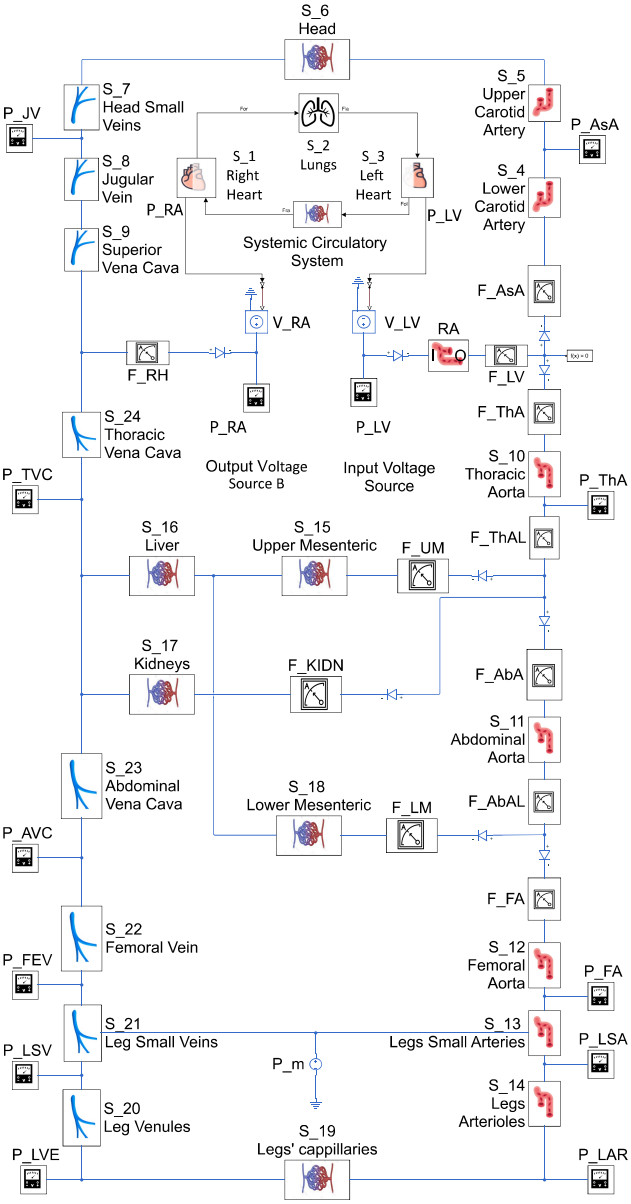

Figure 3: Block scheme in Matlab/Simulink.

The design of the system in Fig. 3 is implemented with the circuit elements specified in [19] after their conversion of centimetre–gram–second system (CGS) to international system (SI) units, as given in Table 1. In this implementation, we assume that the human body is in horizontal position, where the impact of gravity and leg muscle contractions produced by walking or activities like standing up is avoided. Through these values, the blood pressure graph derived in Fig. 4 is obtained, which accounts for standard metrics in the HCS [8].

2.2 Markov model of the HCS

Considering the flow of nanobots in the HCS, they present different trajectories as they complete a loop. For instance, a given

Body Region		State	Circuit Elements				
			R_1 [Ω]	R_2 [Ω]	R_3 [Ω]	C [μF]	L [H]
Arteries	LCA	S_4	20	–	–	167	–
	UPC	S_5	30	–	–	167	–
	ThA	S_{10}	15	–	–	208	–
	AbA	S_{11}	15	–	–	83.4	–
	FA	S_{12}	25	–	–	83.4	–
	LSA	S_{13}	40	–	–	83.4	–
	LAR	S_{14}	60	–	–	250	–
Capillaries	HEAD	S_6	6400	–	–	–	–
	UM	S_{15}	5100	300	–	8000	–
	LIV	S_{16}	700	–	–	5100	–
	REN	S_{17}	7000	500	–	2100	–
	LM	S_{18}	46000	400	–	1300	–
	LCAP	S_{19}	8000	–	–	–	–
Veins	HSV	S_7	500	–	–	450	–
	JV	S_8	88	5.73	–	378	0.789
	SVC	S_9	535	10.11	–	62.3	0.032
	LVE	S_{20}	600	3000	–	–	–
	LSV	S_{21}	600	9000	–	–	–
	FEV	S_{22}	40	9000	28	835	2.82
	AVC	S_{23}	40	0.83	–	170	0.164
	TVC	S_{24}	76	0.63	–	1000	0.089

Table 1: Values of the circuit elements in SI units [19].

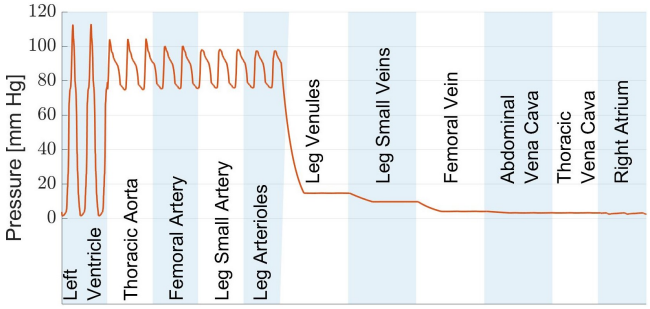

Figure 4: Blood pressure in the different portions of the circulatory system when a person is lying in the horizontal position.

nanobot situated in the left heart randomly jumps to the carotid (upper body) or the thoracic aorta according to the bifurcation in this region (Fig. 1). This random location of the nanobot, driven by the blood flow, may be modeled as a discrete stochastic process to account for their positions in the HCS. Furthermore, we assume the Markov property concerning independent transitions

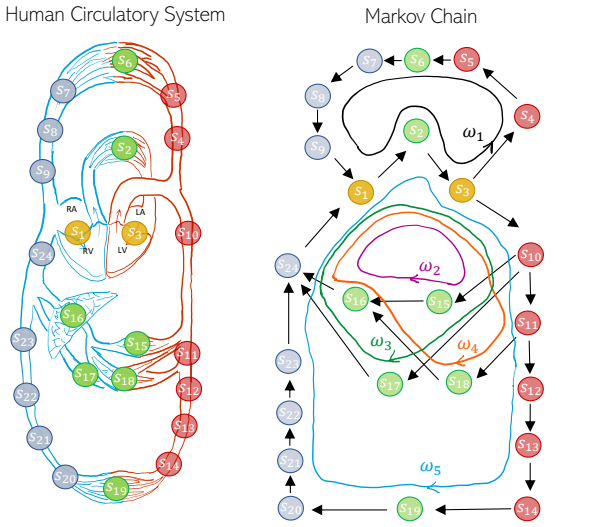

Figure 5: Markov model and its equivalent circuits' representation.

produced in the bifurcations regarding the previous locations of the nanobot. That is, the transitions are only dependent on the flow properties locally to the bifurcation. In this respect, the location of the nanobots may be modeled through a Markov chain where each state corresponds to their position in the HCS [6].

Considering the different segments represented through S_1 to S_{24}, regarding the electric model in the HCS represented in Fig. 2, a Markov model is similarly conceived with equivalent stages as shown in Fig. 5. In the Markov model, the stages represent the location of a given nanobot traveling through the blood in the HCS. By this model, a nanobot that is located on the right heart next jumps to the lungs, then to the left heart, to the arteries, to the capillaries, and finally to the veins, following the blood flows as a closed circuit in the HCS.

2.3 Deriving the transition probabilities of the Markov chain

Considering the diagram for the Markov model in Fig. 5, a variety of transition probabilities are already given due to the direct connections between stages. For instance, it is certain that a nanobot jumps from the head (S_6) to the head small vein segment (S_7), resulting to a transition probability of one. Excluding these direct connections, the probabilities to determine in this diagram corresponds to the following transitions: $S_3 \rightarrow S_4$, $S_3 \rightarrow S_{10}$, $S_{10} \rightarrow S_{11}$, $S_{10} \rightarrow S_{15}$, $S_{10} \rightarrow S_{17}$, $S_{11} \rightarrow S_{12}$, and $S_{11} \rightarrow S_{18}$.

To determine these probabilities, we rely on the equivalent representation of the Markov model through its closed-circuit representation [11]. In this equivalent representation, the connection between stages in the Markov chain may be represented by oriented closed circuits of weights ω_i, as depicted in Fig. 5 through ω_1 to ω_5. This equivalent circuit representation models a particle traveling through a given circuit that randomly changes the circuit at the interceptions [14].

For a valid representation, each stage in the Markov chain must be connected with at least one circuit of strictly positive weight ω_i, where the equivalence of both representations is given by the relation between the transition probabilities and the coefficients ω_i. A given transition probability regarding $S_i \rightarrow S_j$ is the ratio of the sum of coefficients of circuits connecting the stages S_i to S_j, to the sum of all the coefficients regarding the circuits that pass through S_i. To illustrate, the transition probability regarding $S_3 \rightarrow S_4$ is given by

$$p_{3,4} = \frac{\omega_1}{\sum_{i=1}^{5} \omega_i}. \tag{1}$$

Alternatively, considering the electric-circuit representation of the HCS in Fig. 3, it can be also represented by their electric-current flows (current mesh) [9] through the loops determined by the ω_i-circuits in Fig. 5. That is, the circuit in Fig. 3 can be solved by meshing the currents in loops equivalent to those defined by the ω_i-circuits in Fig. 5. The corresponding current's mesh provides a metric for the electric-circuit loop as the coefficient ω_i is the metric that characterizes the circuit loop in the Markov chain. Furthermore, similar to the assumption regarding the circuit representation of the Markov chain, where a traveling particle randomly changes its circuit path, in the electric circuit a similar case happens in the interceptions for equivalent particles driven by the current flow.

In this respect, the representation of the ω_i-circuits in Fig. 5 plays the same role as the representation of the electric-current flows in Fig. 3. Using this analogy, the numerator in Eq. (1), given by ω_1, represents the current flow in the loop passing through the blocks S_4→S_5→S_6→S_7→S_8→S_9→S_1 →S_2→S_3 in Fig. 3, while the denominator is the current through the branch with the block F_LV, which in turn accounts for all electric current flows in the circuit. Similarly, the numerator and denominator in Eq. (1) is directly given by the current sensor blocks F_AsA and F_LV in Fig. 3, respectively, as

$$p_{3,4} = \frac{I_{\text{F\_AsA}}}{I_{\text{F\_LV}}}, \tag{2}$$

where the time-dependent representation has been omitted for brevity, and $I_{\text{F\_AsA}}$ and $I_{\text{F\_LV}}$ are the corresponding current flows assumed to be strictly positive (due to the connection of diodes in this interception and the strictly positive voltage in P_LV). Similarly, the remaining transition probabilities can be determined considering their corresponding currents yielding

$$\begin{aligned} p_{3,10} &= \frac{I_{\text{F\_ThA}}}{I_{\text{F\_LV}}}, \quad p_{10,11} = \frac{I_{\text{F\_AbA}}}{I_{\text{F\_ThAL}}}, \quad p_{10,15} = \frac{I_{\text{F\_UM}}}{I_{\text{F\_ThAL}}}, \\ p_{10,17} &= \frac{I_{\text{F\_KIDN}}}{I_{\text{F\_ThAL}}}, \quad p_{11,12} = \frac{I_{\text{F\_LM}}}{I_{\text{F\_AbAL}}}, \quad p_{11,18} = \frac{I_{\text{F\_FA}}}{I_{\text{F\_AbAL}}}. \end{aligned} \tag{3}$$

These relations provide the equivalent representation of the HCS through the Markov model in Fig. 5 and their electric-circuit in Fig. 3. Given the transition probabilities in (2) and (3), and considering that those direct connections have a transition probability equal to one, and the non-connected nodes have a transition probability equal to zero, then the transition matrix of their corresponding Markov chain can be directly derived as $\Pi = \{p_{i,j}\}$.

Based on the transition matrix Π, a variety of metrics can be computed to study the location and the dynamics of nanobots when traveling through the HCS. The location of a given nanobot can be determined (in a probabilistic sense) through the stationary probability vector $\boldsymbol{\nu}$ after solving the linear equation $\boldsymbol{\nu} = \boldsymbol{\nu}\Pi$. According to $\boldsymbol{\nu}$, the probability that a nanobot is located on a given stage S_i is directly given by the corresponding vector-element ν_i. Furthermore, considering a total of N nanobots, on average the total of nanobots on a given state S_i can be also computed as $\nu_i N$.

The trajectory of a given nanobot can be assessed by computing the probability to travel through the different circuits represented in Fig. 5. For instance, the probability to travel through the weighted circuit ω_1 is given by the product regarding all the concerned transition probabilities as $p_{1,3} \cdot p_{2,3} \cdot p_{3,4} \cdot p_{4,5} \cdot p_{5,6} \cdot p_{6,7} \cdot p_{7,8} \cdot p_{8,9} \cdot p_{9,1}$, and similarly for the other loops.

2.4 The BloodVoyagerS Simulation Framework

The BloodVoyagerS simulator framework [7] derives the location per nanobot in the HCS according to the achievable speed per vessel segment. The most recent solution accounts for the main regions connected through the vessels as depicted in Fig. 6. Loops are realised through the two arms and legs separately, along with the main tissues in the head, the thorax, and the lower body region.

To enable comparative results regarding the Markov chain model, we implement in the BloodVoyagerS simulator framework a similar HCS structure by identifying the components in common. The originally 94 vessels and structures of BloodVoyagerS are merged to account for the similar regions in the Markov chain model. Fig. 6 illustrates how the 94 vessels are mapped to the 24 stages in Fig. 2. For instance, the *thoracic vena cava* and the arteries in the arms are fused in the BloodVoyagerS framework to account for S_{10} in Fig. 2. Arteries are also merged in both legs to account for S_{20} to S_{22}, and a similar procedure is applied with the veins and capillaries as represented in Fig. 6.

3 RESULTS AND DISCUSSION

Nanobots travel through the several loops in the HCS following the blood flow and randomly jump to different segments in the bifurcations. To characterize their movement we conducted Matlab®[1]-based simulations in Simulink according to the electric-circuit in Figures 2 and 3. Based on this scheme, we obtained the electric currents to determine the transition probabilities in Equations (2) and (3).

Fig. 7 illustrates the derived transition probabilities after time-averaging the relations in Equations (2) and (3). Major differences in the transition probabilities are obtained in the case of S_3 and S_{11}. According to the transitions in S_3, it is more likely to travel to the thoracic and lower body than to the upper body, as expected considering the total of regions in the lower body. The same happens at the bifurcation at S_{11}, it is more probable to travel to the legs (in the direction of S_{12}) than to the lower mesenteric bed (S_{18}).

For the five loops illustrated in Fig. 5, the resulting passage probabilities are represented in Fig. 8. As expected, the most vital circuits (ω_1, ω_2, ω_3, ω_5) are similarly probable to be passed through, except for loop ω_4 concerning the lower mesenteric bed as a direct consequence of the high impedance represented in the analog circuit (given by the resistor value R_1 in S_{18} Table 1).

[1]MATLAB is a registered trademark of The MathWorks, Inc.

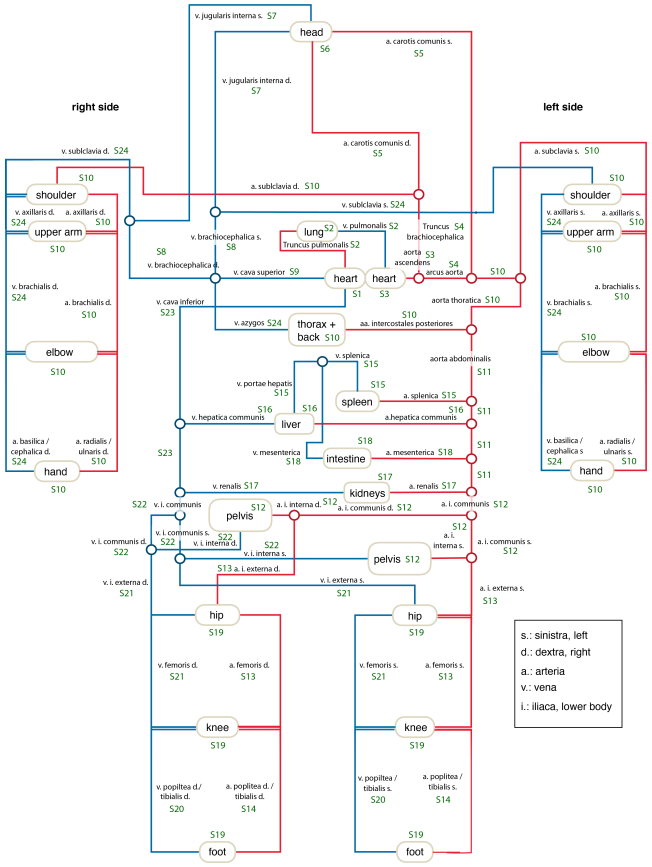

Figure 6: HCS as represented in the BloodVoyagerS simulation framework with mapping to the Markov model segments indicated in green.

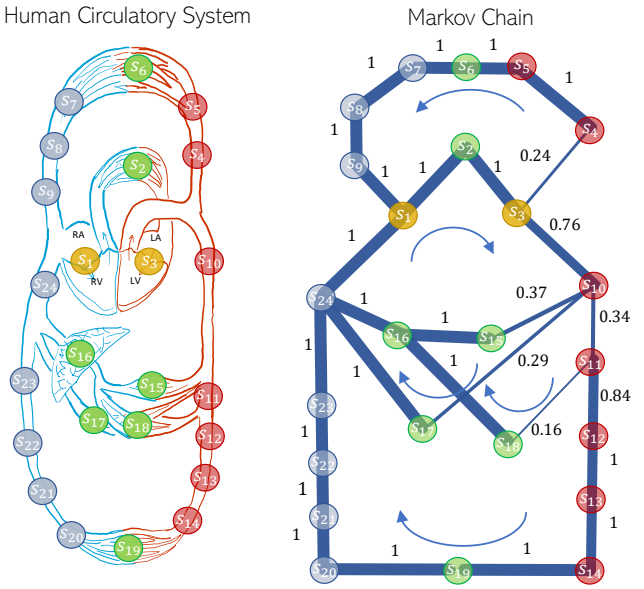

Figure 7: Graph with transition probabilities represented in the width of edges.

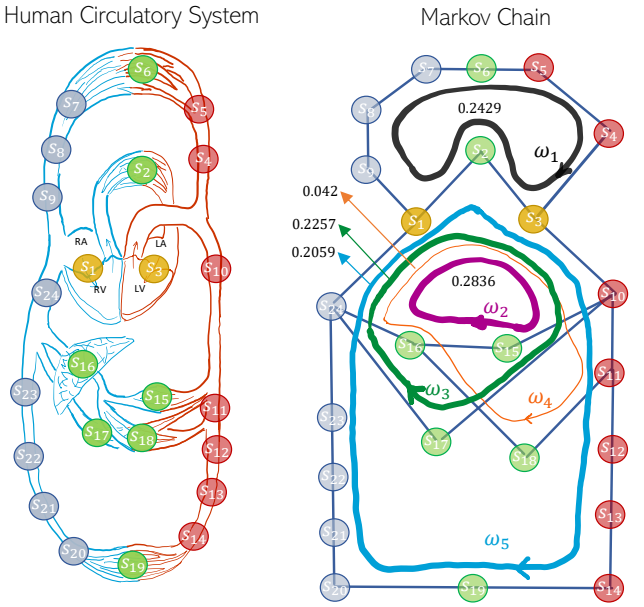

Figure 8: Graph with loops probabilities represented in the width of the loops.

Finally, Fig. 9 illustrates the location probabilities of nanobots per body region modeled by the Markov chain and the BloodVoyagerS simulator when analyzing the flow of 1000 nanobots. Some regions exhibit a high correspondence regarding the location of nanobots, some others exhibit a different distribution. Differences are mainly produced due to the different topologies and the resulting parameters, represented by the Markov model in Fig. 5 and the BloodVoyagerS in Fig. 6.

However, considering both results, most frequently visited regions are in agreement with the superposition of the different closed loops in the HCS. Provided that the heart and lungs are linked to all loops, they are visited more by the nanobots. The next most frequented segments are the *Thoracic Aorta* and *Vena Cava*. These vessel segments are also linked to all loops except for ω_1. The remaining regions are equally frequented (except for the lower mesenteric) with a probability of about 30 percent of the most frequented regions.

4 CONCLUSION

The presented analysis provides an overview of the possibilities to implement a passive drug delivery system in the HCS by means of injected nanobots. Considering the derived results, nanobots injected in the HCS are equally distributed in the most vital circuits around the body. The most frequented regions are the heart, lungs, as well as the *thoracic aorta*, and the *vena cava*, which is in correspondence with the regions that comprise the largest blood flow. Remaining regions are similarly frequented (except for the lower mesenteric) with a probability of about 30 percent of the main regions. This balance on the presence of nanobots in the HCS provides the basis to analyze the status update to account for their

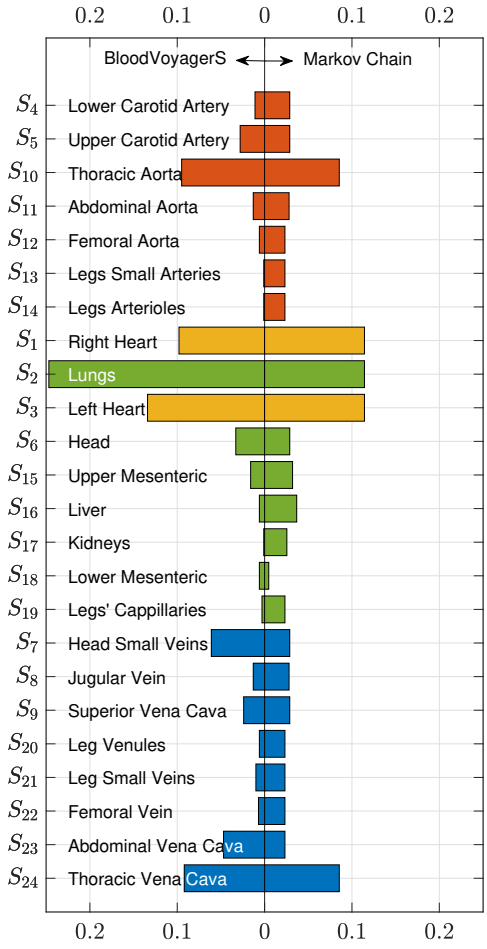

Figure 9: Distribution of nanobots in the circulatory system.

monitoring as a future research. The results presented were derived through the analogies between the circuit representation of the Markov chain and the electric circuit representation, both for the HCS. A more detailed description can be provided by increasing the total number of segments in the region of interest without a prohibitive complexity due to the reduced representation of the electric models. Although the transition probabilities here illustrated are derived from average flows in the HCS, the analysis can be extended to consider the time-dependent variability of the blood flow. Finally, to account for the traveling time between segments (concerning delay) the different stages of the Markov chain mostly represent the same delay path. The delay paths should be in correspondence with the blood speed on each segment, and those segments with the larger speed will account for a lower number of Markov stages. This derivation will be also part of a future study.

ACKNOWLEDGMENTS

Reported research was supported in part by the project MAMOKO funded by the German Federal Ministry of Education and Research (BMBF) under grant numbers 16KIS0917 and by the project NaBoCom funded by the German Research Foundation (DFG) under grant number DR 639/21-1. We thank for the revision of this work to MD. Serguei Torres Miranda, Pediatric Echo Lab, Duke Children Hospital, Durham, North Caroline, USA. We also thank for the valuable discussion concerning the electric circuit representations to Jorge Luis González Rios, Interdisciplinary Centre for Security, Reliability and Trust (SnT), University of Luxembourg, Luxembourg.

REFERENCES

[1] Ian F. Akyildiz, Massimiliano Pierobon, S. Balasubramaniam, and Y. Koucheryavy. 2015. The Internet of Bio-Nano Things. *IEEE Communications Magazine (COMMAG)* 53, 3 (March 2015), 32–40. https://doi.org/10.1109/MCOM.2015.7060516

[2] David J Brayden. 2003. Controlled release technologies for drug delivery. *Drug Discovery Today* 8, 21 (Nov. 2003), 976–978. https://doi.org/10.1016/s1359-6446(03)02874-5

[3] Youssef Chahibi, Massimiliano Pierobon, Sang Ok Song, and Ian F. Akyildiz. 2013. A Molecular Communication System Model for Particulate Drug Delivery Systems. *IEEE Transactions on Biomedical Engineering* 60, 12 (Dec. 2013), 3468–3483. https://doi.org/10.1109/tbme.2013.2271503

[4] Yifan Chen, Panagiotis Kosmas, Putri Santi Anwar, and Limin Huang. 2015. A Touch-Communication Framework for Drug Delivery Based on a Transient Microbot System. *IEEE Transactions on NanoBioscience* 14, 4 (June 2015), 397–408. https://doi.org/10.1109/tnb.2015.2395539

[5] Falko Dressler and Stefan Fischer. 2015. Connecting In-Body Nano Communication with Body Area Networks: Challenges and Opportunities of the Internet of Nano Things. *Elsevier Nano Communication Networks* 6 (June 2015), 29–38. https://doi.org/10.1016/j.nancom.2015.01.006

[6] Constantine Gatsonis, James S. Hodges, Robert E. Kaas, and Nozer D. Singpurwalla. 2012. *Case Studies in Bayesian Statistics*. Vol. II. Springer Science & Business Media.

[7] Regine Geyer, Marc Stelzner, Florian Büther, and Sebastian Ebers. 2018. BloodVoyagerS: Simulation of the Work Environment of Medical Nanobots. In *5th ACM International Conference on Nanoscale Computing and Communication (NANOCOM 2018)*. ACM, Reykjavík, Iceland, 5:1–5:6. https://doi.org/10.1145/3233188.3233196

[8] Arthur C. Guyton and Michael. E. Hall. 2015. *Guyton and Hall Textbook of Medical Physiology* (14 ed.). Elsevier.

[9] William Hayt, Jack Kemmerly, Jamie Phillips, and Steven Durbin. 2019. *Engineering Circuit Analysis* (9 ed.). McGraw-Hill Education, New York City, NY.

[10] Zhe Hu. 2001. HSP. https://de.mathworks.com/matlabcentral/fileexchange/818-hsp

[11] Sophia L. Kalpazidou. 2006. *Cycle Representations of Markov Processes*. Springer. https://doi.org/10.1007/0-387-36081-6

[12] Otilia M. Koo, Israel Rubinstein, and Hayat Onyuksel. 2005. Role of nanotechnology in targeted drug delivery and imaging: a concise review. *Nanomedicine: Nanotechnology, Biology and Medicine* 1, 3 (Sept. 2005), 193–212. https://doi.org/10.1016/j.nano.2005.06.004

[13] Anke Kuestner, Lukas Stratmann, Regine Wendt, Stefan Fischer, and Falko Dressler. 2020. A Simulation Framework for Connecting In-Body Nano Communication with Out-of-Body Devices. In *7th ACM International Conference on Nanoscale Computing and Communication (NANOCOM 2020)*. ACM, Virtual Conference. https://doi.org/10.1145/3411295.3411308

[14] J. MacQueen. 1981. Circuit Processes. *The Annals of Probability* 9, 4 (Aug. 1981). https://doi.org/10.1214/aop/1176994365

[15] Tadashi Nakano, Tatsuya Suda, Y. Okaie, M. J. Moore, and A. V. Vasilakos. 2014. Molecular Communication Among Biological Nanomachines: A Layered Architecture and Research Issues. *IEEE Transactions on NanoBioscience* 13, 3 (Sept. 2014), 169–197. https://doi.org/10.1109/TNB.2014.2316674

[16] Paul K. Newton, Jeremy Mason, Kelly Bethel, Lyudmila A. Bazhenova, Jorge Nieva, and Peter Kuhn. 2012. A Stochastic Markov Chain Model to Describe Lung Cancer Growth and Metastasis. *PLOS ONE* 7, 4 (April 2012), e34637. https://doi.org/10.1371/journal.pone.0034637

[17] Vincent C. Rideout. 1991. *Mathematical and Computer Modeling of Physiological Systems*. Prentice Hall, Upper Saddle River, NJ.

[18] Yubing Shi, Patricia Lawford, and Rodney Hose. 2011. Review of Zero-D and 1-D Models of Blood Flow in the Cardiovascular System. *BioMedical Engineering OnLine* 10, 1 (2011), 33. https://doi.org/10.1186/1475-925x-10-33

[19] M. F. Snyder and V. C. Rideout. 1969. Computer Simulation Studies of the Venous Circulation. *IEEE Transactions on Biomedical Engineering* BME-16, 4 (Oct. 1969), 325–334. https://doi.org/10.1109/tbme.1969.4502663